Calculation and analysis of gamma-induced irradiation damage cross section

Shengli Chen[a,b,*], David Bernard[a], Cyrille De Saint Jean[a]

[a] CEA, Cadarache, DEN/DER/SPRC/LEPh, 13108 Saint Paul Les Durance, France
[b] Université Grenoble Alpes, I-MEP2, 38402 Saint Martin d'Hères, France

A B S T R A C T

Due to the discrepancies of gamma-induced Displacement per Atom (DPA) cross sections among different calculations, the present work identifies the sources of the discrepancies and recommends the computation of displacement cross sections induced by photons, including the stopping power for electrons and positrons, the differential scattering cross sections, and the gamma-matter interactions. The production of electrons and positrons and the corresponding gamma-induced damage cross sections computed with the above methods are validated against Monte Carlo simulations. The damage cross section for Photoelectric Effect (PE) is negligible for incident photon energy higher than 2 MeV. Above 2 MeV, the percentage of atomic displacement for Compton Scattering (CS) decreases with incident energy, while that for Pair Production (PP) increases and becomes more important than CS above 10 MeV. In the PP, it is recommended to differently treat positrons and electrons for damage calculations because positrons produce 68–77% of DPA induced by electrons. 9.8×10^{-10} DPA/year gamma-induced displacement is obtained in the heavy reflector of PERLE experiment using the recommended damage cross sections. Neglecting the influence of moderator on photon flux in reflector, 8.1×10^{-4} DPA/year gamma-induced displacement damage is found in the reflector of Evolutionary Pressurized Reactor (EPR).

1. Introduction

The irradiation-induced displacement damage is one of the most important factors that influence the features of materials. The atomic displacement damage is conventionally quantified by the number of Displacement per Atom (DPA). In nuclear reactors, neutron and gamma are two main sources to produce the displacement damage of materials. Assuming the standard DPA metric, the neutron-induced DPA cross sections can be computed by the processing code NJOY [1]. Moreover, some improvements for computing the neutron-induced DPA cross sections are recently suggested [2,3]. The resonance self-shielding correction on neutron-induced DPA rate calculation is also studied [4]. Results in Ref. [4] show that the consideration of self-shielding can reduce about 10% neutron-induced DPA rate in the fuel cladding of the ASTRID [5] inner core.

Alexander and Rehn [6,7] showed that the gamma-induced DPA in the Reactor Pressure Vessel (RPV) of an Advanced Boiling Water Reactor (ABWR) is around 50% or even more of the DPA induced by neutrons. Due to the smaller water gap between the reactor core and the RPV for Pressurized Water Reactors (PWRs), the slowing down and absorption of neutrons are less important than those in Boiling Water Reactors (BWRs). Because of the less important slowing down of

neutrons, comparing with the neutron-induced DPA, the gamma-induced displacement damage is relatively less important in PWRs than that in BWRs. However, because of the importance of DPA for the study of nuclear materials, the gamma-induced DPA should be thoroughly studied in both PWRs, BWRs, Fast Reactors (FRs), and fusion reactors.

The methods to compute gamma-induced DPA cross sections are firstly proposed by Oen and Holmes in 1959 [8]. Gamma-ray produces the displacement damage through the three gamma-matter interactions, which are Compton Scattering (CS), Photoelectric Effect (PE), and Pair Production (PP). The gamma-matter interactions produce electrons (and positrons for the PP) which induce the atomic displacement by collision with atoms in materials. Therefore, the electron (and positron)-induced DPA should be investigated for computing the gamma-induced damage. Oen computed fast electron-induced DPA cross sections for various isotopes with different threshold energies of atomic displacement in 1973 [9]. Oen's electron-induced DPA cross sections are based on the Mott's differential cross section [10] and the Kinchin-Pease (KP)-DPA formula [11]. Using the Oen's electron-induced DPA cross sections, Baumann computed the gamma-induced DPA in heavy water reactors [12]. Later, Kwon and Motta calculated gamma-induced DPA cross sections for various elements with 24 eV and 40 eV displacement threshold energies [13]. Pinera et al. [14] computed the KP-

DPA based damage cross sections using the Monte Carlo simulations.

By taking the electronic excitation effect into account, Norget-Robinson-Torrens (NRT) [15] proposed a new formula to compute DPA. Consequently, Oen's electron-induced DPA cross sections should be improved. Alexander [16] computed the gamma-induced displacement cross section by accounting the efficiency factor 0.8, which is used in NRT-DPA. However, Alexander consider only the factor 0.8, the electronic energy loss by the recoil atoms is not accounted for (the statement that Alexander used NRT-DPA in page 5 of Ref. [14] is not exact). Fukuya and Kimura [17] used NRT-DPA to compute gamma-induced DPA cross sections for iron.

As plotted in Fig. 5 in Ref. [14], large discrepancies are observed for gamma-induced KP-DPA cross sections among different computations. Therefore, the present work firstly analyzes the different gamma-induced DPA cross sections. Based on the thorough analyses of KP-DPA based displacement cross sections, the methods of gamma-induced DPA cross sections are recommended. Due to the large discrepancies among KP-DPA based gamma-induced displacement cross sections, the recommended results are compared with Fukuya and Kimura [17] to conclude the results of NRT-DPA based atomic displacement cross sections for photons.

With the recommended gamma-induced DPA cross sections, the DPA rate induced by gamma-ray in the heavy reflector of the Programme d'Etude du Réflecteur Lourd dans Eole (PERLE) experiment [18,19] is computed. Assuming the similar gamma spectrum in reflector of Evolutionary Pressurized Reactor (EPR) to that in the PERLE, the gamma-induced DPA rate is estimated for the former. The material for the reflector is Stainless Steel (SS), which is also the material for the RPV, fuel cladding in Fast Reactors (FRs), and a candidate fuel cladding in Accident Tolerant Fuel (ATF) of PWR [20,21]. Since iron is the most abundant element in SS, the DPA rate of iron is studied in the present work.

2. Methods

2.1. Stopping power for electrons and positrons

As mentioned previously, the gamma induces displacement damage through the produced electrons (and positrons for PP) through the gamma-matter interactions. To study the electron and positron-induced reactions, the stopping power is required. The stopping power is defined as:

$$S(E) = -dE/dx \tag{1}$$

where E is the energy of the incident particle, x stands for the penetration in the matter. Fig. 1 shows various electronic stopping power in iron.

The Bethe's formula [22] is the most classical. The Bethe-Ashkin [23] stopping power is used by Oen and Holmes [8]. Cember's formula [24] has similar results as the Bethe-Ashkin and is used by Kwon and Motta [13]. Baumann took the Seltzer-Berger [25] stopping power to compute the gamma-induced DPA in heavy water reactors [12]. Differences are evident among the above-mentioned stopping powers. The International Commission on Radiation Unit and measurements (ICRU) compiled stopping power for electrons and positron in various materials [26]. It is observed in Fig. 1 that the ICRU recommended electronic stopping power is much larger than the previous 4 stopping powers at high energies. The main reason is that the bremsstrahlung is more important at high energy, while only the collision effect is accounted for in the above analytic stopping powers. The ICRU stopping power is used by Fukuya and Kimura [17].

Because the ICRU stopping powers include both collision and radiative (bremsstrahlung) effects, it is recommended to take the compiled data in the ICRU report [26]. However, the stopping power of positron is not given for iron. Fukuya and Kimura [17] deduced the collision stopping power of iron based on the assumption that the ratio
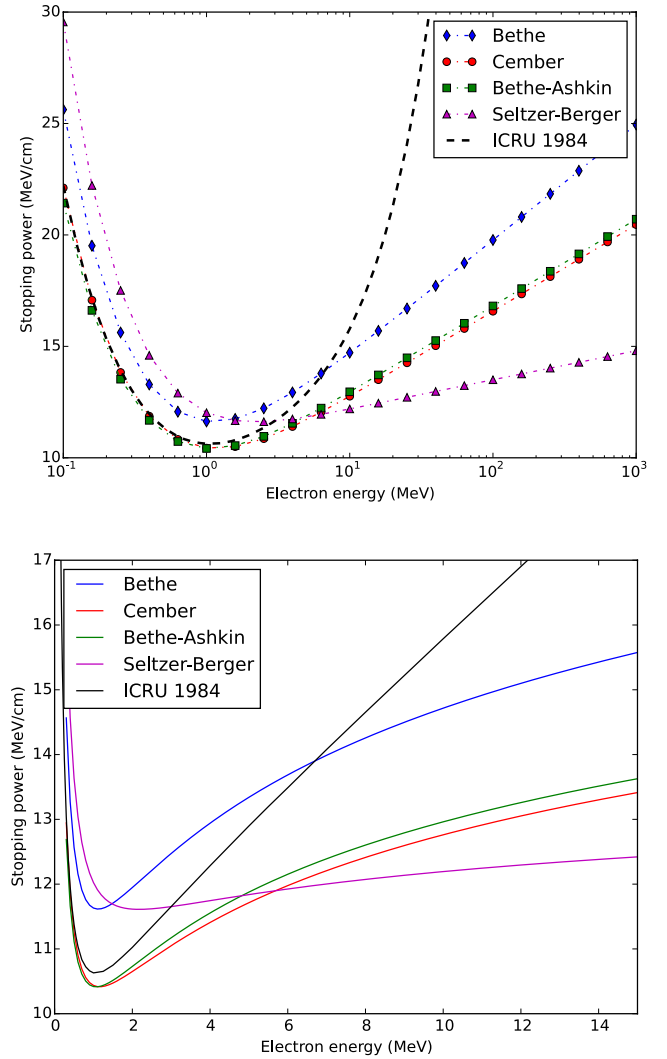

Fig. 1. Different electronic stopping power in iron. The energy in the upper figure is plotted on a linear scale and that in the lower is plotted on a logarithmic scale.

of collision stopping power of positron to electron is constant (so the ratio computed for copper can be used for iron). The present work uses the assumption made by Fukuya and Kimura. More accurate results can be obtained using Eqs. (2.17) and (2.18) in Ref. [26]. For the radiative stopping power, ICRU assumed that the ratio of the electron to positron depends only on E/Z^2 (Z is the atomic number) [26]. Therefore, the ratio of copper is used to compute the radiative stopping power of positrons in iron.

Fig. 2 shows the ratios of collision and radiative stopping power for copper based on ICRU data. The vertical dashed line represents the threshold displacement energy, which is presented in Section 2.2. Because the ratio for collision is almost constant in the considered region, the constant value 0.97 is used. For the radiative stopping power, the point-wise ratios and linear-log interpolation between two points are used.

2.2. Electron and positron-induced DPA cross sections

The total DPA cross section by an incident electron or positron of energy E is calculated by:

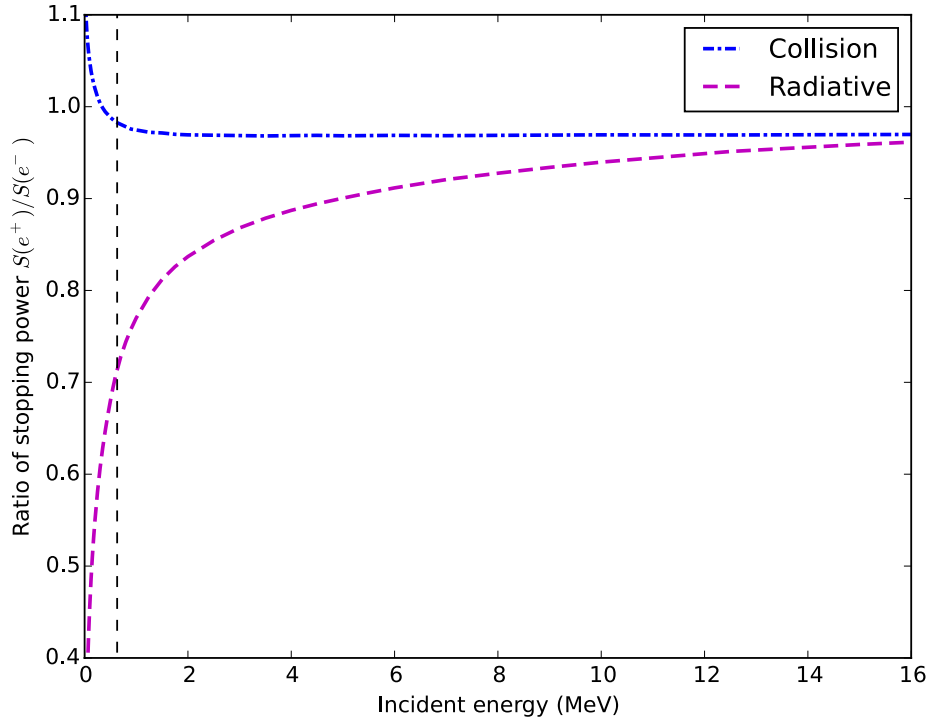$$\sigma(E) = \int_0^{T_m} \nu(T) \frac{d\sigma}{dT} dT \tag{2}$$

Fig. 2. Ratio of stopping power of positron to that of electron for copper [26]. The vertical dashed line represents the threshold displacement energy.

where $d\sigma/dT$ is the differential scattering cross section, T_m is the maximum energy that can be transferred to atom, $\upsilon(T)$ is the number of atomic displacements induced by an atom with energy T. Oen computed tabulated values of electronic $d\sigma/dT$ for various elements with Mott's [10] differential scattering cross section. McKinley and Feshbach [27] deduced an approximation with a simpler expression for the differential scattering cross section:

$$\frac{d\sigma}{dT}(E, T) = \frac{\pi Z^2 e^4 (1 - \beta^2) T_m}{(mc^2)^2 \beta^4 T^2} \left\{ 1 - \beta^2 \frac{T}{T_m} \pm \frac{\pi}{137} \beta Z \left[\left(\frac{T}{T_m} \right)^{1/2} - \frac{T}{T_m} \right] \right\}$$

(3)

where $\beta^2 = E(E + 2mc^2)/(E + mc^2)^2$ with mc^2 is the rest energy of electron or positron, Z is the atomic number, the term involving $\pi \beta Z/137$ is positive for electron and negative for positron. Accordingly, the differential scattering cross section of electron is larger than that of positron. The maximum transferred energy is:

$$T_m(E) = \frac{2E}{Mc^2}(E + 2mc^2)$$

(4)

where Mc^2 is the rest energy of atom. According to Eq. (4), the threshold energy of electrons or positrons for displacing atoms is:

$$T_d^{e,p} = \sqrt{(mc^2)^2 + Mc^2 E_d/2} - mc^2$$

(5)

where E_d is the threshold energy of atomic displacement. The typical value of E_d for iron is 40 eV [28]. Using this value for iron or ^{56}Fe, one can obtain $T_d^{e,p} = 0.63$ MeV.

The classical KP-DPA [11] points out:

$$\upsilon(T) = \begin{cases} 0, & T < E_d \\ 1, & E_d < T < 2E_d \\ T/2E_d & T > 2E_d \end{cases}$$

(6)

for Primary Knock-on Atom (PKA) energy below the ionization energy. Taking the electronic excitation into account, the NRT-DPA [15] formula is expressed by:

$$\upsilon(T_a) = \begin{cases} 0, & T_a < E_d \\ 1, & E_d < T_a < 2.5E_d \\ 0.8T_a/2E_d & T_a > 2.5E_d \end{cases}$$

(7)

where T_a is the damage energy that available to produce atomic displacement. By interpreting Lindhard's results [29], Robinson deduced the analytic formula as [30]:

$$T_a(\varepsilon) = T/[1 + k(3.4008\varepsilon^{1/6} + 0.40244\varepsilon^{3/4} + \varepsilon)]$$

(8)

where $\varepsilon = T/E_L$ with $E_L = 86.931 Z^{7/3}$ eV, $k = 0.133745 Z^{2/3} A^{-1/2}$, Z and A are the atomic number and the atomic mass number, respectively.

Oen applied Mott's differential scattering cross section and KP-DPA formula to compute the DPA cross section for electrons [9]. The present work recalculates the electronic DPA cross sections with the same differential cross section and DPA formula. Fig. 3 shows the Oen's numerical results and our calculations. The close to unity values of the ratio of recomputed DPA to Oen's results validate our calculations and the accuracy of Oen's data. The difference in the energy range below 1 MeV is mainly due to the limited significant digit of tabulated data in Ref. [9].

Oen gave only the numerical results of Mott's differential scattering cross sections for electron. In order to use the same law of differential cross sections for electron and positron, the McKinley-Feshbach approximation given by Eq. (3) is proposed. Fig. 4 points out the electronic DPA cross sections computed by McKinley-Feshbach approximation and Mott's exact results and the differences on DPA cross sections. Small difference is found between the DPA cross sections computed with McKinley-Feshbach formula and those obtained with Mott's formalism. Consequently, the McKinley-Feshbach approximation is used in the present work. The correspondence between McKinley-Feshbach approximation and Monte Carlo simulations is shown in Section 2.3.4.

Taking the McKinley-Feshbach approximation, the NRT-DPA formula based DPA cross sections for electrons and positrons are illustrated in Fig. 5. The positron-induced DPA cross sections are smaller than the electron-induced DPA cross sections. Therefore, one should individually consider positrons for investigating the positron-induced DPA cross sections, whereas most works treat a positron as an electron
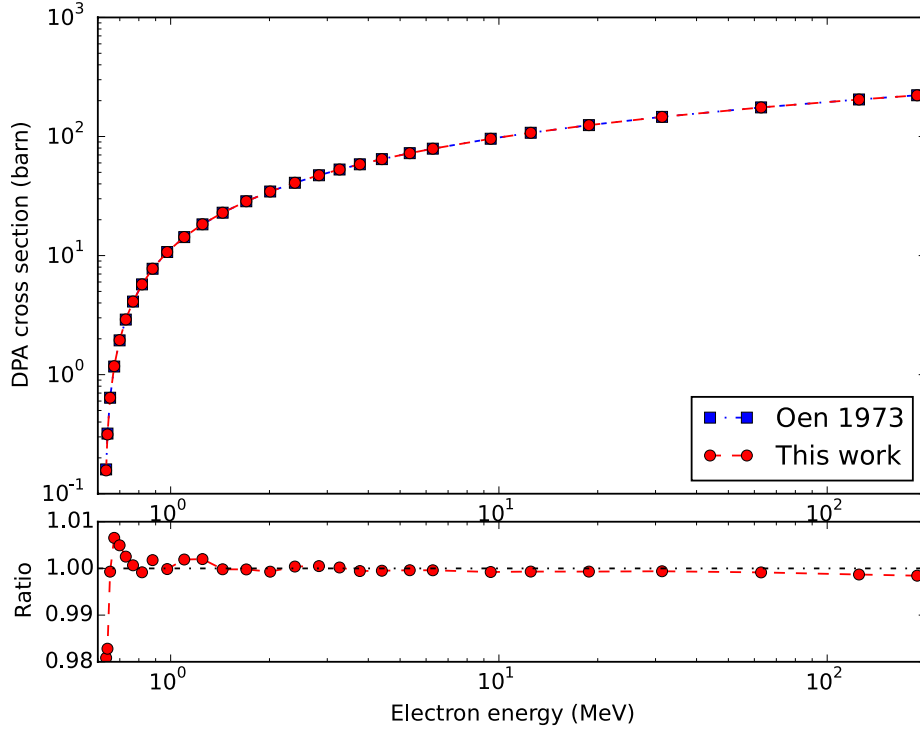
Fig. 3. Electron-induced DPA cross sections based on KP-DPA.

to compute gamma-induced DPA through the PP mechanism.

2.3. Gamma-induced DPA cross sections

Total gamma-induced DPA cross section is the sum of three partial damage cross sections:

$$\sigma_t(E_\gamma) = \sigma_{CS}(E_\gamma) + \sigma_{PE}(E_\gamma) + \sigma_{PP}(E_\gamma) \tag{9}$$

2.3.1. Compton scattering

The DPA cross section for CS is given by [8]:

$$\sigma_{CS}(E_\gamma) = \int_0^{E_{max}} \frac{d\sigma^{CS}(E_\gamma, E)}{dE} n(E) dE \tag{10}$$

where $d\sigma^{CS}(E_\gamma, E)/dE$ is the CS cross section for producing an electron of energy E. For convenience, the subscript (superscript resp.) of CS, PE, and PP refers to the damage (photon reaction resp.) cross section. The Klein-Nishina formula [31] shows:
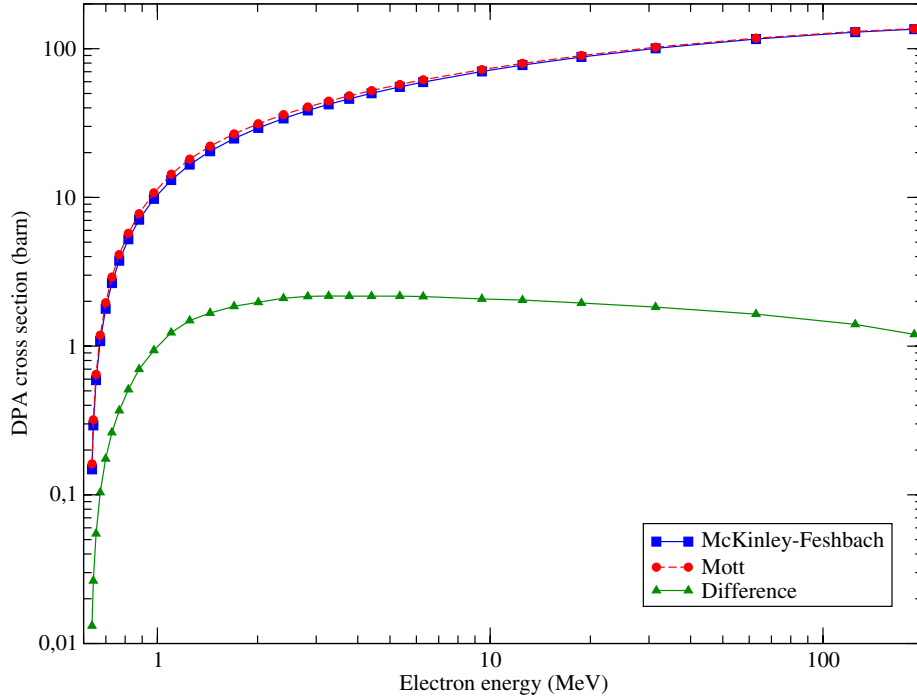

Fig. 4. Electron-induced NRT-DPA cross sections based on McKinley-Feshbach and Mott scattering cross sections.
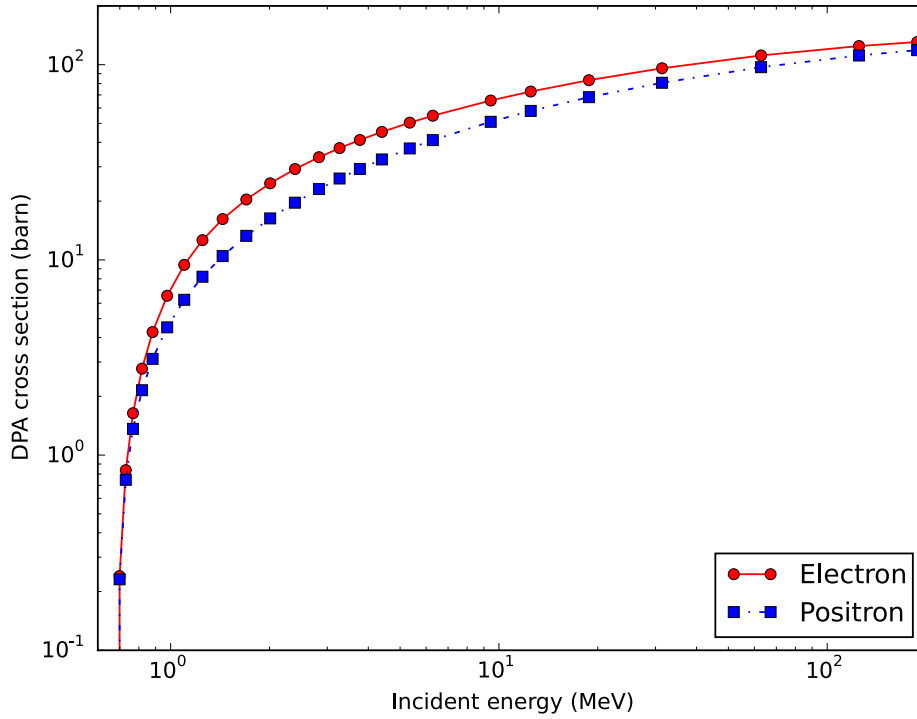
Fig. 5. Electron and positron-induced NRT-DPA cross sections for iron.

$$\frac{d\sigma^{CS}(E_\gamma, E)}{dE} = \frac{\pi(9\times10^3 e)^2 Z}{mc^2(E_\gamma - E)^2}\left\{\left(\frac{mc^2 E}{E_\gamma^2}\right)^2 + 2\left(\frac{E_\gamma - E}{E_\gamma}\right)^2\right.$$
$$\left. + \frac{E_\gamma - E}{E_\gamma^3}[(E - mc^2)^2 - (mc^2)^2]\right\} \quad (11)$$

where e is the charge of electron 1.602×10^{-19}C, all energies are in MeV and $d\sigma^{CS}(E_\gamma, E)/dE$ is in m^2/MeV = 10^{28}barn/MeV. The upper limit of integration represents the maximum kinetic energy of electrons induced by a gamma ray of energy E_γ and is given by:

$$E_{max}(E_\gamma) = \frac{2E_\gamma}{2 + mc^2/E_\gamma} \quad (12)$$

$n(E)$ in Eq. (10) represents the average number of displaced atoms induced by an electron with kinetic energy E. It is computed with:

$$n(E) = N_V \int_0^E \frac{\sigma^e(T)}{S(T)}dT \quad (13)$$

where N_V is the atomic density of the material, S is the electronic stopping power, and σ^e refers to the electron-induced DPA cross section studied in Section 2.2. $n(E)$ is shown in Fig. 6 with the red solid line.

2.3.2. Photoelectric effect

The kinetic energy of electrons produced by PE is:

$$E = E_\gamma - B_e \quad (14)$$

where B_e is the binding energy of electrons. B_e is generally of the order of magnitude of several hundred eV, which is very small compared with E_γ. Fukuya and Kimura took the value of 711 eV for K-shell electrons of iron [17], while most studies neglect the electronic binding energy. Due to the determined energy of electrons for a given energy photon, the damage cross section for PE is:

$$\sigma_{PE}(E_\gamma) = \sigma^{PE}(E)n(E) \quad (15)$$

In the region of damage calculation, the DPA cross section for PE is given by Hall's formula [32]:

$$\sigma^{PE}(E) = \frac{5}{4}\frac{4\pi Z(9\times10^3 e)^2\alpha^4}{(mc^2)^2}\exp[-\pi\alpha + 2\alpha^2(1 - \ln\alpha)]$$
$$\times \frac{(\gamma + 1)^{3/2}}{(\gamma - 1)^{7/2}}\left\{\frac{4}{3} + \frac{\gamma(\gamma - 2)}{\gamma + 1}\left[1\right.\right.$$
$$\left.\left. - \frac{1}{2\gamma\sqrt{\gamma^2 - 1}}\ln\left(\frac{\gamma + \sqrt{\gamma^2 - 1}}{\gamma - \sqrt{\gamma^2 - 1}}\right)\right]\right\} \times 10^{28} \text{ barn} \quad (16)$$

where the factor 5/4 accounts the PE for electrons of K-shell and other shells (1/4 of K-shell), $\alpha = Z/137$, γ is the Lorentzian factor

$$\gamma = \frac{E + mc^2}{mc^2} \quad (17)$$

and $\beta = \sqrt{1 - 1/\gamma^2}$.

It is noticeable that Fukuya and Kimura [17] forgot the exponential in PE cross section. In Ref. [8], Oen and Holmes used energy in mc^2 unit and omitted the factor $4\pi e^4$. Kwon and Motta [13] took the same equation as Oen and Holmes, but there is a error in the second line of Eq. (5): the denominator should be E_γ^4 rather than E_γ^2.

2.3.3. Pair production

For the PP, because both electrons and positrons are produced for a photon with energy high than $2mc^2 = 1.022$ MeV, one should treat both electron-induced and positron-induced displacement damage. Alexander doubled the electron-induced damage for the PP [16]. Kwon and Motta neglected the positron-induced DPA because the positron annihilate by combining with an electron [13]. Fukuya and Kimura used the most reasonable method that computing the positron-induced damage with the same method applied in the calculation of electron-induced DPA by using the corresponding stopping power for positrons [17]. This work recommends the utilization of the method proposed by Fukuya and Kimura.

Similar to the computation of DPA cross sections for CS given in Eq. (10), the PP damage cross section is calculated by:

$$\sigma_{PP}(E_\gamma) = \int_0^{E_\gamma - 2mc^2} \frac{d\sigma^{PP}(E_\gamma, E)}{dE}[n(E_\gamma - 2mc^2 - E) + \bar{n}(E)]dE \quad (18)$$
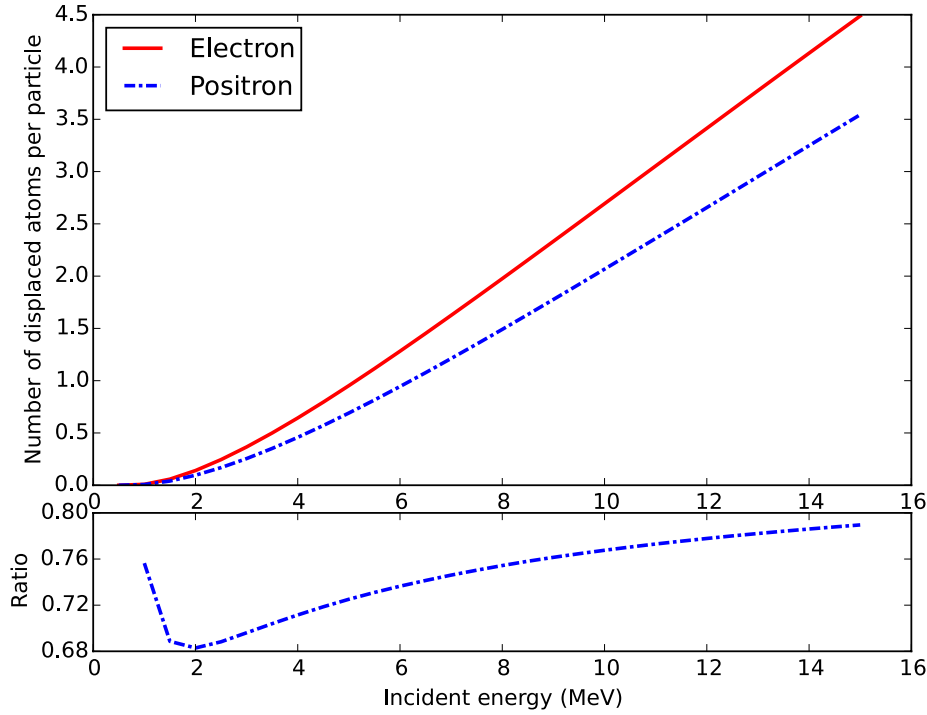
Fig. 6. Total displaced atoms per incident electron or positron. The lower figure shows the ratio of displacement induced by positron to that induced by electron.

where $\bar{n}(E)$ represents the average number of displaced atoms induced by a positron with kinetic energy E. $\bar{n}(E)$ is illustrated in Fig. 6 with the blue dotted line. The ratio $\bar{n}(E)/n(E)$ shown Fig. 6 points out that $\bar{n}(E)$ is 68%-80% of $n(E)$. The differential cross section for the PP $d\sigma^{PP}(E_\gamma, E)/dE$ has been determined by Davisson and Evans [32]. Evans calculated the integration over the whole energy domain [33]. Due to the complexity of differential cross section for PP, Kwon and Motta used Evans' integrated data by assuming the equiprobable energy distribution. There is a typo in Ref. [13] that the constant coefficient in Eq. (12) is 5.8×10^{-4} barn rather than 2.8×10^{-4} barn. Fukuya and Kimura used a numeric approach as:

$$\frac{d\sigma^{PP}(E_\gamma, E)}{dE} = \sigma_{co} Z^2 F(s)/(E_\gamma - 2mc^2) \qquad (19)$$

where $\sigma_{co} = 5.8 \times 10^{-4}$ barn and

$$F(s) = g(u)\left\{ h(u)\left[1 - 2^n\left(s - \frac{1}{2}\right)^n\right] + [1 - h(u)]\left[1 - 2^l\left(s - \frac{1}{2}\right)^l\right]\right\} \qquad (20)$$

where $s = E/(E_\gamma - 2mc^2)$, $u = \ln(E_\gamma/mc^2)$, $l = 2$, $n = 8$, and

$$g(u) = -0.1835u^3 + 1.653u^2 - 2.1543u + 0.7614 \qquad (21)$$

$$h(u) = 0.2193u + 0.1825 \qquad (22)$$

If only the electrons are considered, the damage cross sections for PP computed with Evans' integrated formula and Fukuya-Kimura approximation have a few percent difference. The present work uses the Fukuya-Kimura approximation to consider the energy distribution of electrons and positrons.

2.3.4. Monte Carlo simulations

The approximative analytic expressions of gamma-matter interaction cross sections are proposed to compute the gamma-induced DPA cross sections. To verify the above-mentioned gamma-matter interaction cross sections, the present work compares the analytic expression with Monte Carlo simulated data. The simulations of photon transport are performed with Tripoli-4.10 [34] using the Evaluated Photon Data Library (EPDL)-97 [35].

Fig. 7 illustrates the production of electrons in ^{56}Fe for incident gamma energies of 3 MeV and 15 MeV. The statistical uncertainties of Monte Carlo simulations are plotted in grey (not evident due to the small uncertainties), while the simulated data are illustrated by the red lines. The small peak near to the incident energy is the electron production for PE. Good agreement between the analytic expression and Monte Carlo simulations is found through the production of electrons.

Fig. 8 shows the production of positrons for 3 MeV and 15 MeV incident gamma in ^{56}Fe. Due to the small number of positrons produced by gamma-ray, the statistical uncertainties are larger than those of electron production. The analytic expression has the similar form as the Monte Carlo simulated results. Around 14% difference is observed at the peak of positron production for 3 MeV gamma, whereas the dispersion of simulated data is also about 3%. The tendency shows that the energy distribution of positrons computed with EPDL-97 through Monte Carlo simulations is sharper than that of Fukuya-Kimura. The analytic formula has a globally good agreement with Monte Carlo simulated result for 15 MeV gamma. EPDL-97 has little flatten energy distribution of positrons for gamma-ray with high incident energy. The DPA cross sections computed with the two methods are illustrated in Section 3.4.

3. Results and discussion

3.1. Analyses of gamma-induced DPA cross sections

The methods given in Section 2.3 for computing the gamma-induced damage cross sections are fundamental and common methods. However, as shown in Fig. 5 in Ref. [14], discrepancies are observed among different results. Ref. [14] plots different total DPA cross sections with different threshold energies and different DPA metrics (KP-DPA and NRT-DPA). In order to verifier each calculation, the present work analyzes the partial DPA cross sections.

Fig. 9 plots the DPA cross sections for CS and for electrons of PP computed by Kwon and Motta [13] and those obtained by Baumann [12]. The Baumann's PP results are divided by a factor of 2 because he doubled electron DPA for computing the damage cross sections for PP.
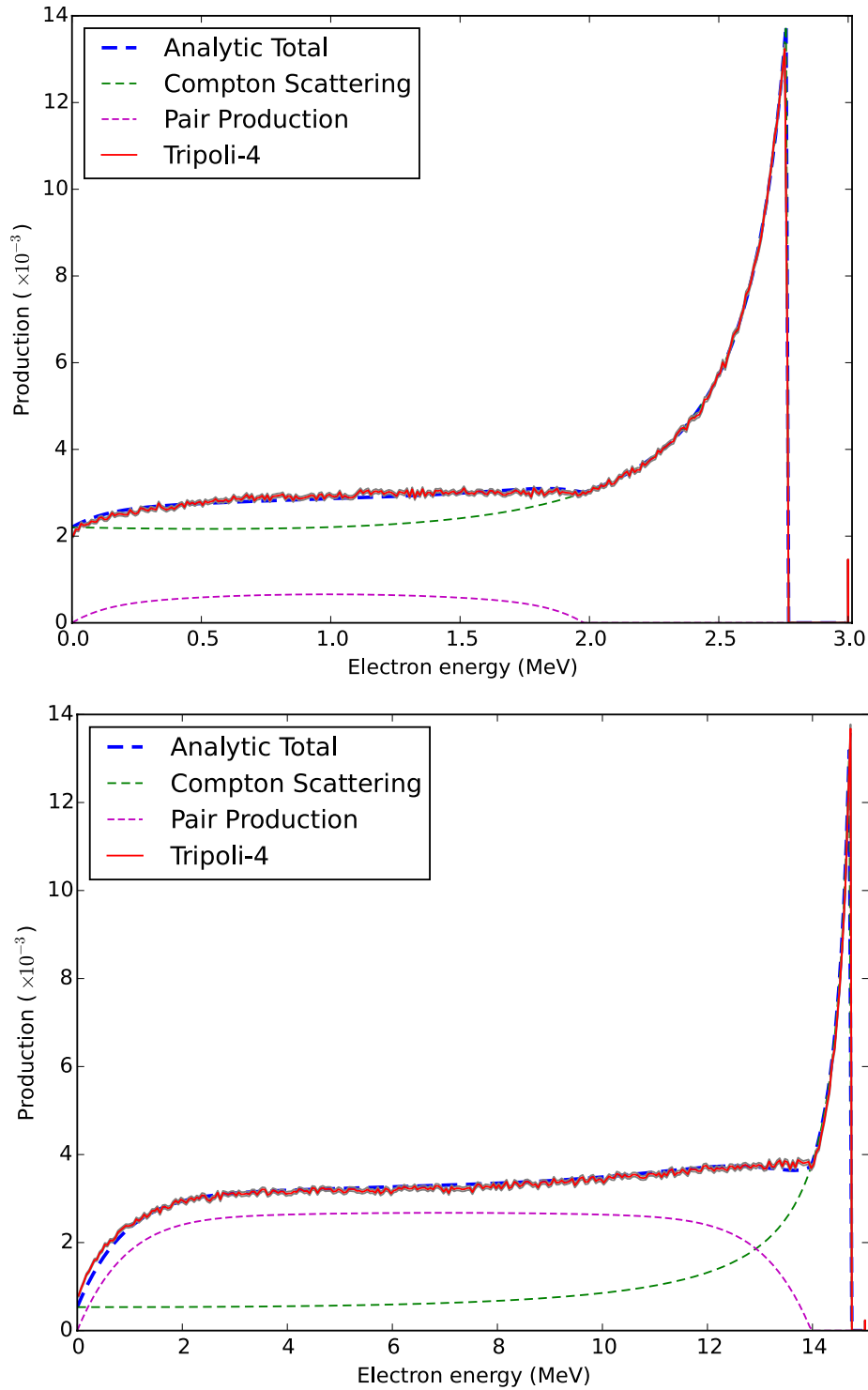
Fig. 7. Electron production of 3 MeV (upper) and 15 MeV (lower) incident gamma.

The Oen's electron-induced damage cross sections are used in both two calculations. The difference is the utilization of different stopping power, Cember [24] by Kwon and Seltzer-Berger [25] by Baumann. Small difference is found in the present work between the damage cross sections computed with the two stopping powers due to the relatively small difference of two stopping powers in [2 MeV, 10 MeV] (shown in Fig. 1). Due to the large discrepancies between Baumann and Kwon, the present work applies the Oen's electronic data and Cember's stopping power to calculate DPA cross sections, which are referred to as Chen in Fig. 9. Our calculations are closer to Baumann's data. Baumann gave

displacement cross section per orbital electron in Ref. [12]. Little difference is found with our results if 25 electrons in CS and 24 electrons in PP are accounted for.

Kwon's data with $E_d = 24$ eV are also quite larger than Fukuya's results with $E_d = 25$ eV. The present work calculates the KP-DPA based gamma-induced displacement cross section with $E_d = 24$ eV and Cember's stopping power (same method used by Kwon) and with $E_d = 25$ eV and ICRU stopping power (same method used by Fukuya). The results are illustrated in Fig. 10. The reproduced DPA cross sections are globally in good agreement with Fukuya's calculations, while quite
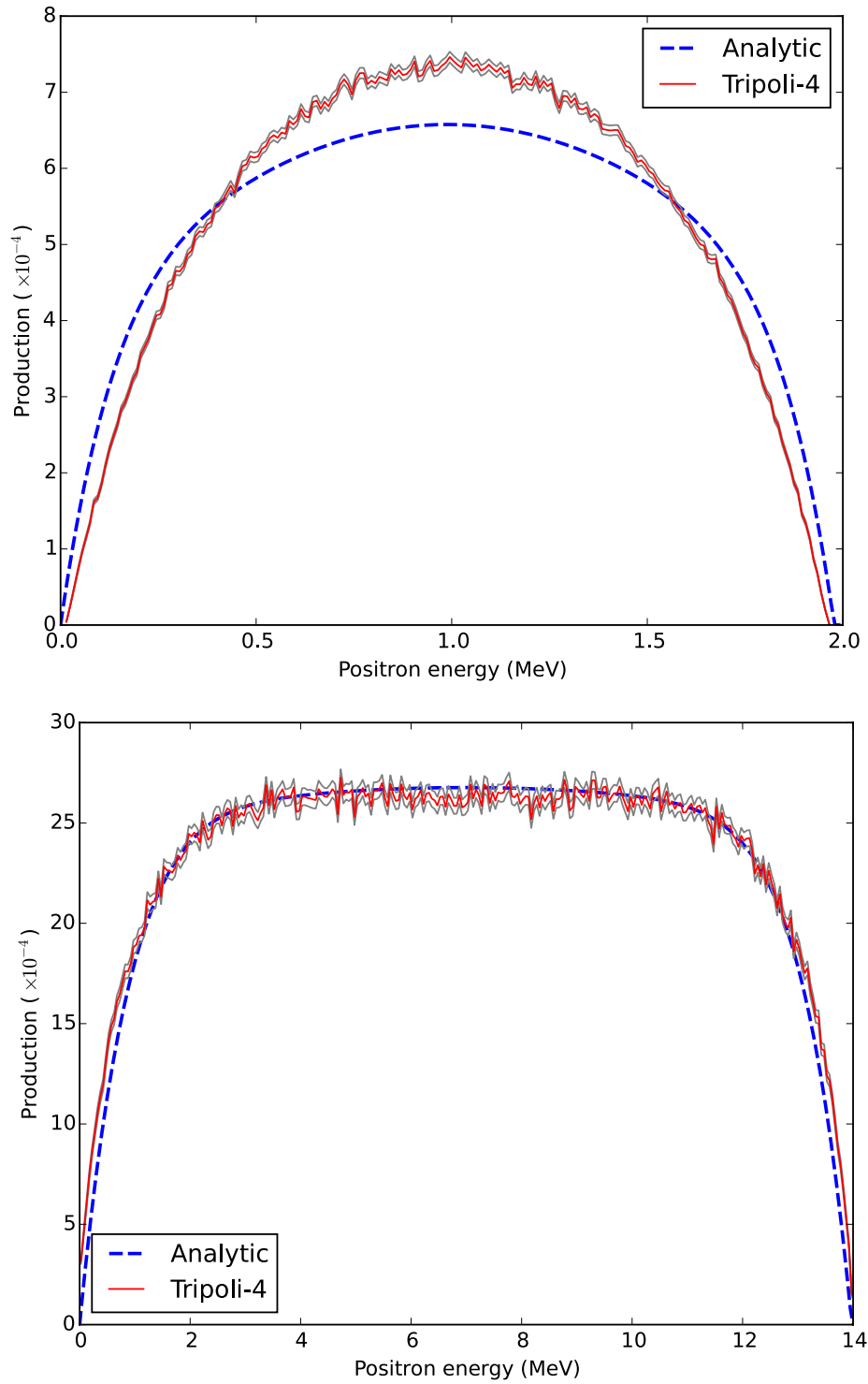
Fig. 8. Positron production of 3 MeV (upper) and 15 MeV (lower) incident gamma.

different results are found with Kwon's results. Both Fig. 9 and Fig. 10 show the stranger tendency of Kwon's calculations for gamma energy of 14 MeV.

The comparisons with Baumann's data $E_d = 40$ eV and the calculations of the present work $E_d = 24$ eV and 40 eV show that Kwon and Motta overestimated gamma-induced displacement cross sections at incident energy below 10 MeV. On the other hand, good agreements are found between our calculations and Baumann's data and Fukuya's KP-DPA results. The gamma-induced damage cross sections based on NRT-DPA metric are shown in Fig. 11 for CS. E_{PKA} vs E_d represents the same

expression as NRT-DPA metric but replacing the damage energy by PKA energy in the judgment of conditions in Eq. (7) [2]. NRT-DPA (Chen) is the standard damage cross section computed and used in the present work. Mott-based NRT refers to the displacement cross section computed with standard NRT-DPA using the Mott's differential scattering cross sections for electrons. The computed gamma-induced damage cross sections correspond with Fukuya's results for CS. In agreement with results shown in Fig. 4, the Mott's scattering cross section gives a little higher displacement damage than McKinley-Feshbach approximation. If PKA energy is used to determine the number of atomic
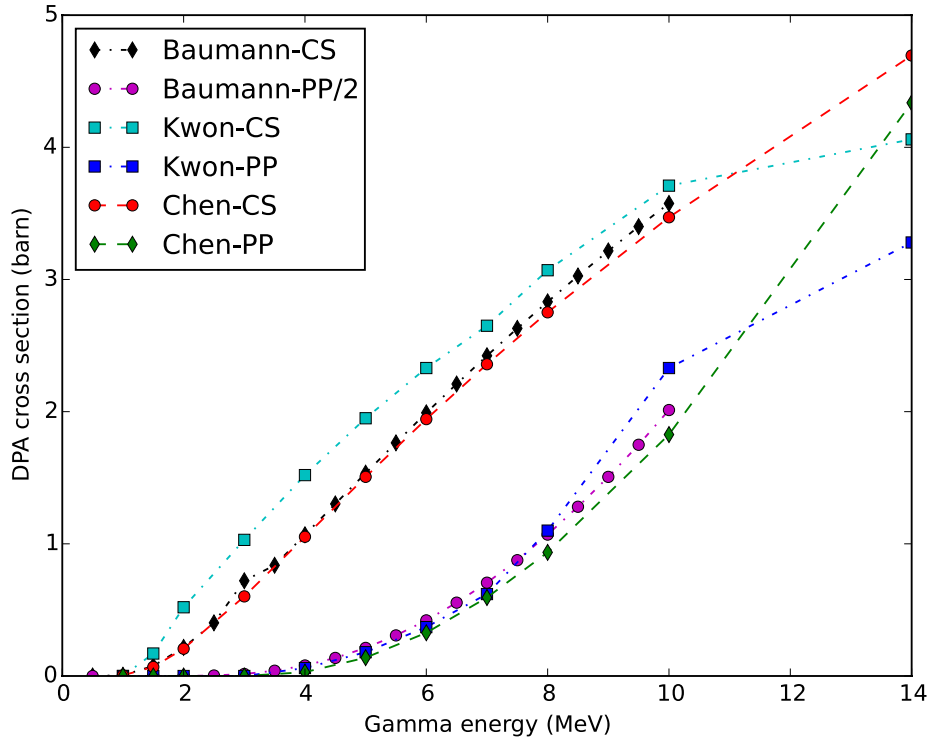
Fig. 9. Gamma-induced KP-DPA (E_d = 40 eV) cross sections for CS and for electrons in PP. Cember's electronic stopping power is used for Kwon and Chen.

displacements in $[E_d, 2.5E_d]$, higher DPA cross sections are obtained due one more displacement for PKA energy larger than E_d but damage energy lower than E_d (1 rather 0 in NRT-DPA).

The gamma-induced damage cross sections for PE are shown in Fig. 12. Comparing with the displacement cross sections for CS and PP, those for PE are negligible. The DPA cross sections for PE are of the order of magnitude of 10^{-3} barn for gamma energy higher than 1 MeV

[13,16]. It should be remarked that Fukuya and Kimura gave DPA cross sections for PE of the order of magnitude of 10^{-4} barn, whereas the present work shows also 10^{-3} barn. It is reasonable that our calculations are a little smaller than Alexander and Kwon because the NRT-DPA metric is used in the present work. In addition, the KP-DPA based Fukuya-Kimura DPA cross sections for PE with $E_d = 25$ eV are also much smaller than the KP-DPA based results with $E_d = 40$ eV
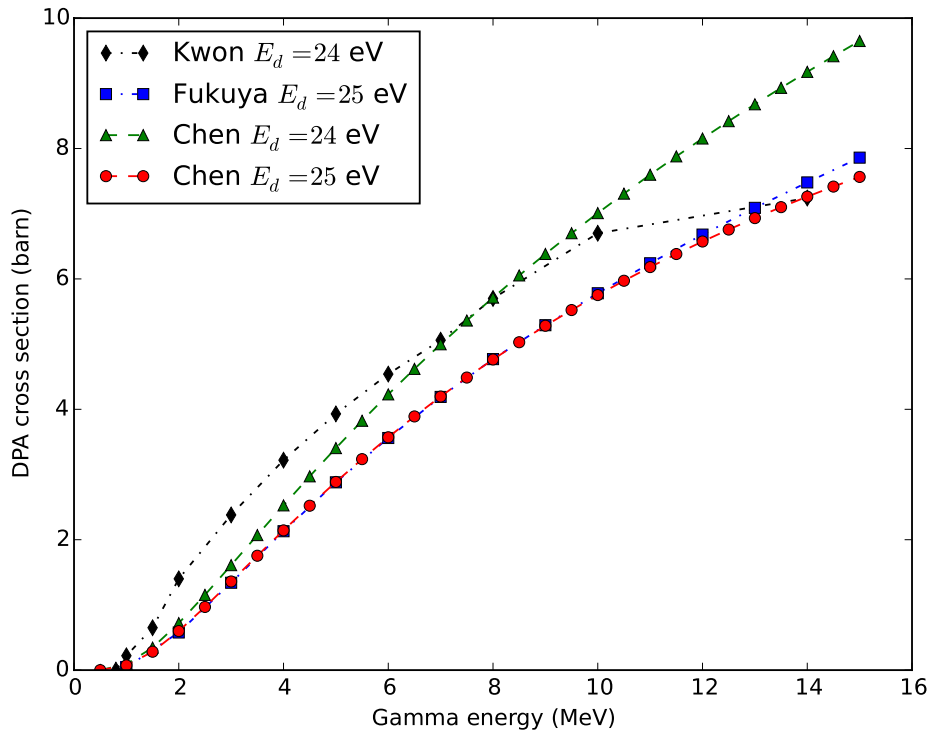

Fig. 10. Gamma CS-induced KP-DPA with various threshold energies cross sections. KP-DPA with E_d = 24 eV are computed with Cember's stopping power which is used by Kwon [13]. KP-DPA with E_d = 25 eV are based on the ICRU stopping power used by Fukuya and Kimura [17].
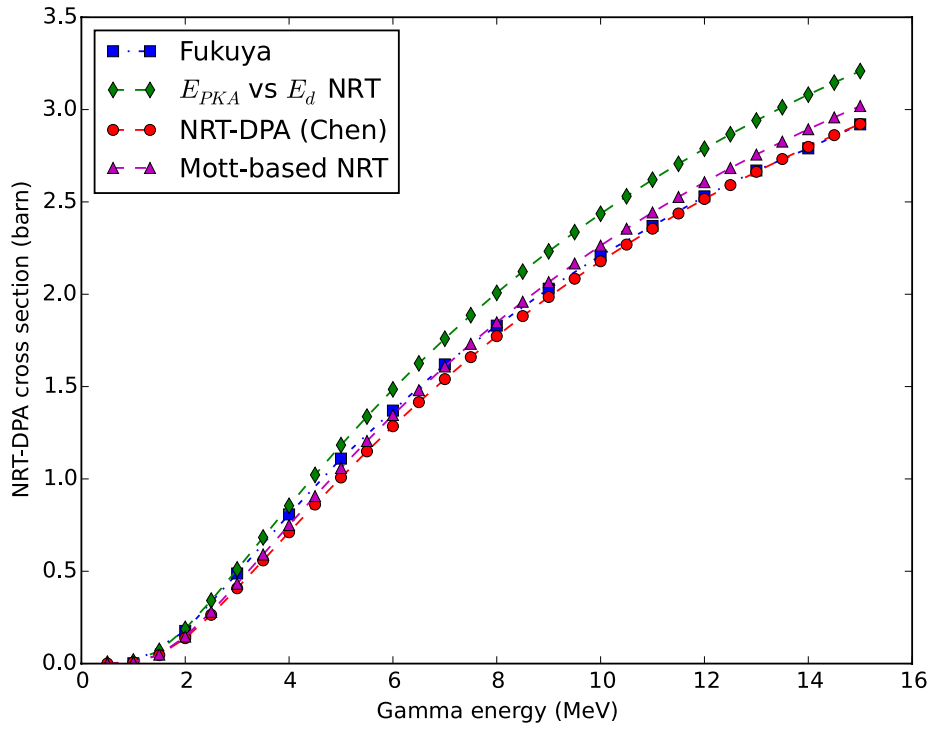
Fig. 11. Gamma CS-induced NRT-DPA (E_d = 40 eV) cross sections.

(Alexander and Kwon) and the NRT-DPA based results with E_d = 40 eV (this work). Therefore, the Fukuya-Kimura DPA cross sections for PE are questionable.

3.2. Comparison with Monte Carlo based results

As explained in Section 2.3.4, the Monte Carlo simulations are used to verify the calculations based on analytic expressions. Using the Monte Carlo simulated production of electrons and positrons, the

gamma-induced DPA cross sections obtained with analytic expressions and those determined with EPDL-97 [35] are shown in Fig. 13. Excellent agreement is found between analytic results and Monte Carlo simulation-based calculations. The only discrepancy is the DPA produced by positrons for gamma energy lower than 3 MeV. The difference can be from statistical uncertainty (as shown in Fig. 8) and the disagreement between Fukuya-Kimura approximation and EPDL-97. Nevertheless, due to the negligible contribution of positron-induced damage in this region, the total gamma-induced DPA cross sections are
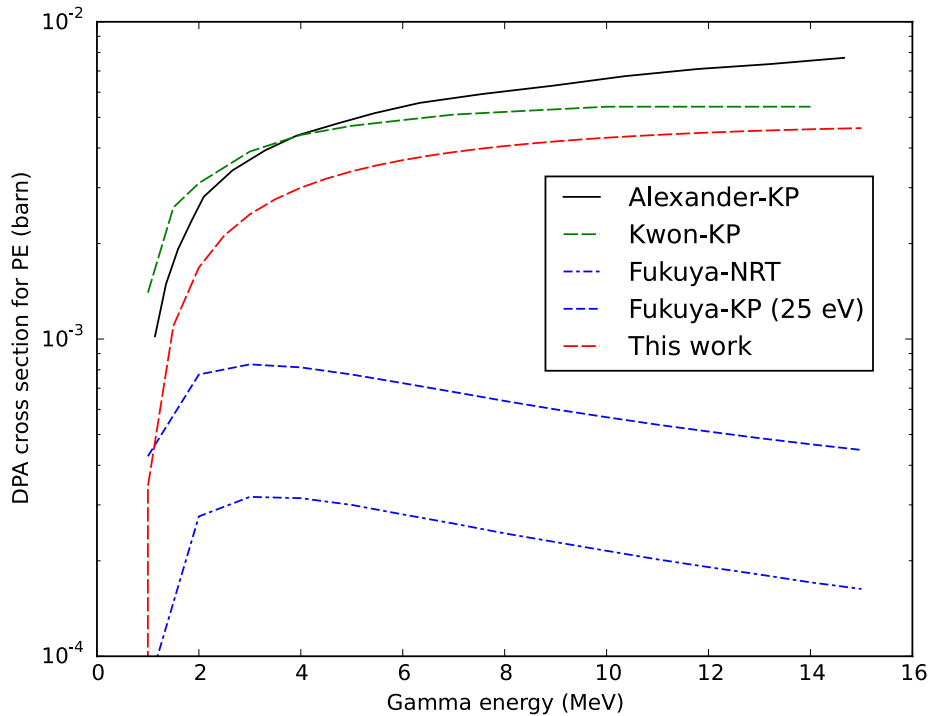

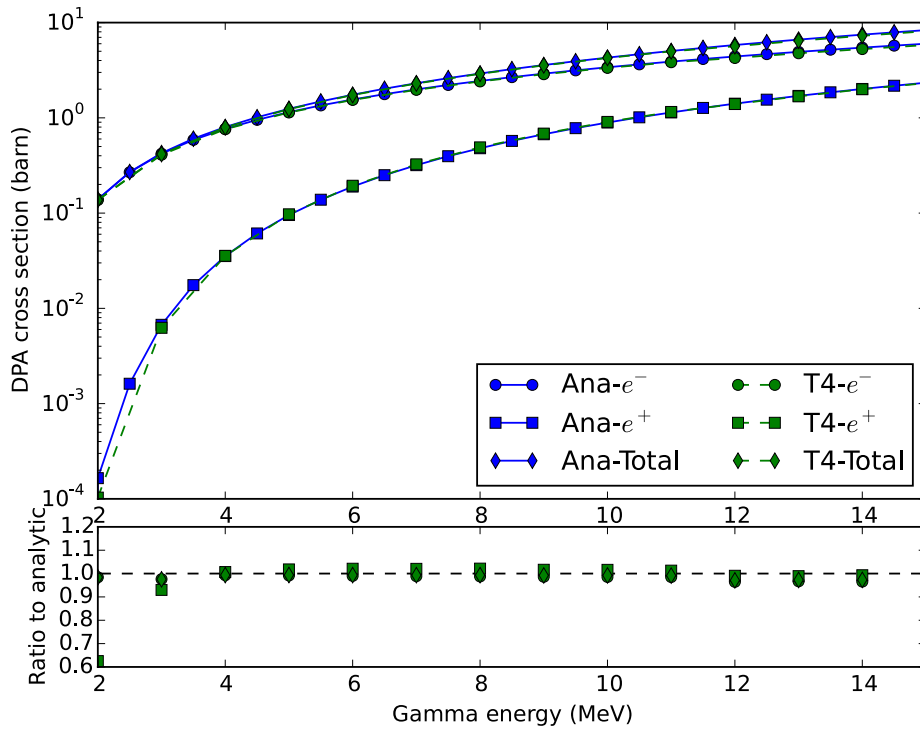**Fig. 12.** Gamma PE-induced DPA (E_d = 40 eV) cross sections.

Fig. 13. Gamma-induced DPA cross sections based on McKinley-Feshbach analytic approximation (blue, noted as Ana) and Tripoli-4 simulations (green, noted as T4). (For interpretation of the references to colour in this figure legend, the reader is referred to the web version of this article.)

the same for both analytic formula and Monte Carlo simulations. By consequence, the computation of gamma-induced DPA cross sections with analytic methods presented in Section 2.3 are validated.

The analytic methods can be used to compute different partial atomic displacement cross sections, such as CS, PE, PP for both electrons and positrons, whereas Monte Carlo simulations show only the productions for electrons and positrons. In addition, Monte Carlo based photon transport requires much time to ensure the convergence of calculations for each incident energy, while the analytic expression can give gamma-induced DPA cross sections in a few seconds. Since the analytic schemes are validated against the Monte Carlos simulations, the former is recommended to perform the computation of gamma-induced atomic displacement cross sections.

3.3. Recommended gamma-induced DPA cross sections

According to the previous analyses, the present work recommends computing gamma-induced DPA cross sections with ICRU stopping power, McKinley-Feshbach approximative electron or positron differential scattering cross section, Hall's formula of PE reaction cross section, Klein-Nishina formula for CS, and Fukuya-Kimura analytic approach for PP. The gamma-induced displacement cross sections for CS, PE, PP, electrons in PP, positrons in PP, and total DPA cross sections are shown in Fig. 14 with the standard NRT-DPA metric. The total gamma-induced DPA cross sections computed by Pinera et al. [14] through Monte Carlo simulations are plotted by scattered points. Because Pinera used KP-DPA metric, it is quite reasonable that his results are a little higher than the NRT-DPA based total cross sections computed in the present work (red curve in Fig. 14).

Fig. 15 illustrates the percentage of each reaction and the ratio of positron-induced to electron-induced displacement in PP mechanism. With results shown in Fig. 14 and Fig. 15, one can conclude that the displacement through the PE is negligible for gamma energy higher than 2 MeV. CS is more (less resp.) important than PP for producing atomic displacement for gamma energy below (above resp.) 10 MeV. In the PP, the displacements produced by positrons are 68–77% of those

induced by electrons, which is in agreement with Fukuya and Kimura [17].

3.4. Gamma-induced DPA in PERLE and EPR

With the gamma-induced displacement cross sections, one can compute gamma-induced DPA rate in each facility through the corresponding gamma flux. The present work takes the heavy reflector in PERLE experiment as an example. The gamma spectrum in the reflector is computed with Tripoli-4 using JEFF-3.1.1 [36] and EPDL-97 and shown in Fig. 16.

Because of the threshold energy of atomic displacement (given by Eq. (5) and shown with dashed line in Fig. 16), 53.6% photons have no contribution on atomic displacement. The statistical uncertainties of the gamma spectrum for Monte Carlo simulation is controlled within 1% below 10 MeV. Above 10 MeV, the statistical uncertainties are higher (2.5% in [10 MeV, 11 MeV] and 16% above 14 MeV) due to the small number of photons. However, due to the small quantities of photons, the influence on DPA rate is very limited. The gamma-induced total DPA rate in the heavy reflector of PERLE is 8.4×10^{-11} DPA/year with 0.1% relative uncertainty. Because of the limit influence of moderator on the photon spectrum, the gamma spectrum in the reflector of EPR should be similar to that in the heavy reflector of the PERLE. According to the ratio of thermal power of EPRs to PERLE (10 W), the gamma-ray produces 8.1×10^{-4} DPA/year average atomic displacement damage in the reflector of EPR, while that induced by neutron is 0.31 DPA/year. Therefore, the gamma-induced DPA is negligible in the heavy reflector, which encloses the reactor core.

4. Conclusions

The calculation of gamma-induced atomic displacement cross sections depends on the DPA metric, stopping power for electrons and positrons, differential scattering cross sections, and gamma-matter interactions. Due to the discrepancies of gamma-induced DPA cross sections among different calculations, the present work identifies the
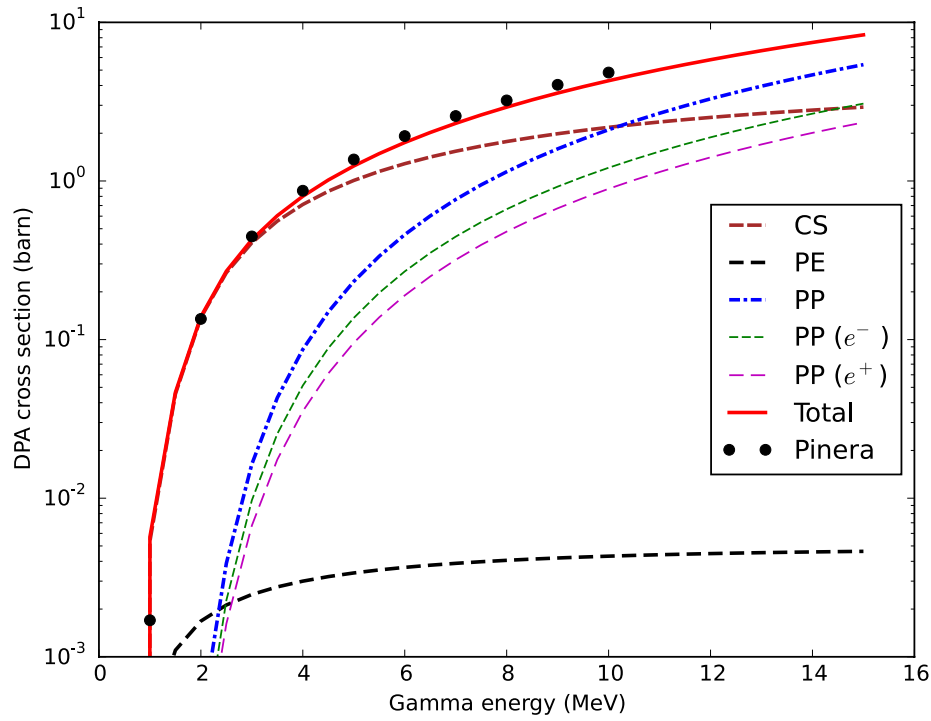
Fig. 14. Gamma-induced NRT-DPA cross sections based on McKinley-Feshbach approximation for iron.

sources of the discrepancies and recommends the computation of displacement cross sections induced by photons. The recommended method using the NRT-DPA metric, ICRU stopping power, Mckinley-Feshbach approximation of differential scattering cross sections for electrons and positrons, Klein-Nishina formula for CS, Hall's formula for PE, and Fukuya-Kimura analytic approach for PP. The production of electrons and positrons and the corresponding gamma-induced damage

cross sections computed with the above methods are validated against Monte Carlo simulations.

The damage cross section for PE is negligible for incident photon energy higher than 2 MeV. However, it is important to remark that the Fukuya-Kimura results for PE are questionable, while their methods and results for CS and PP are quite good. Above 2 MeV, the percentage of atomic displacement for CS decreases with incident energy, while that
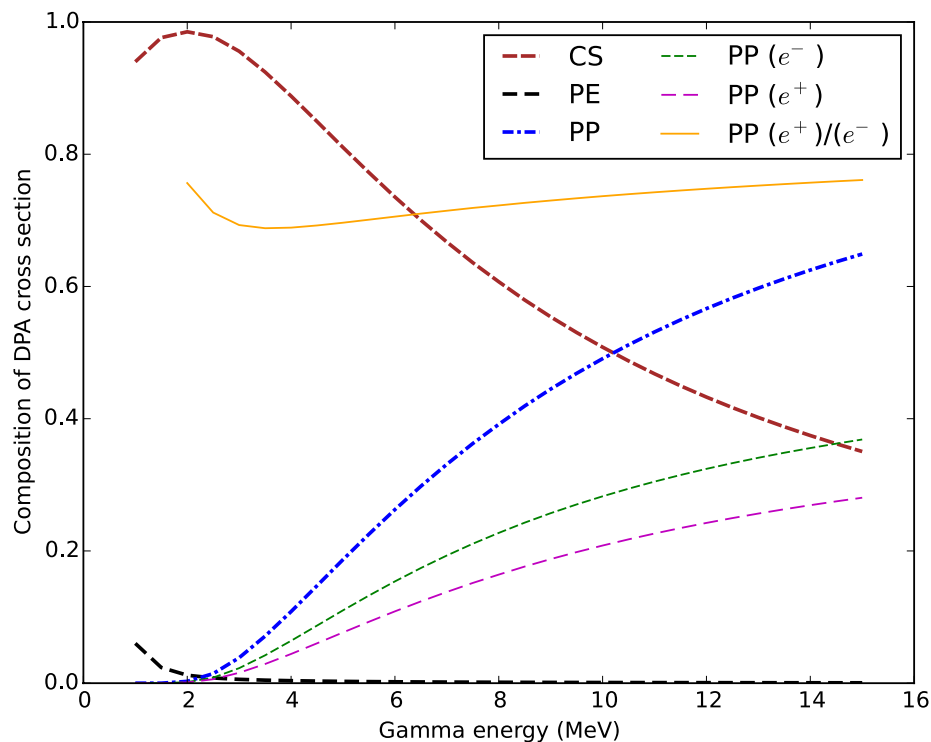

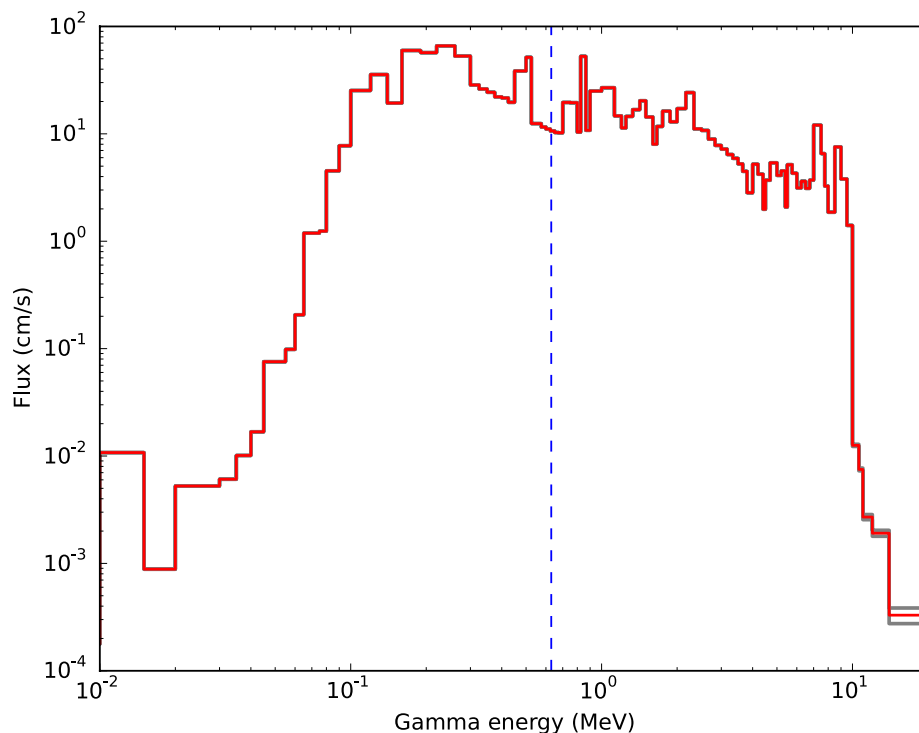**Fig. 15.** Composition of gamma-induced NRT-DPA cross sections.

Fig. 16. Gamma flux in the heavy reflector of PERLE. The grey lines represent the statistical uncertainties. The dashed blue line indicates the threshold of atomic displacement. (For interpretation of the references to colour in this figure legend, the reader is referred to the web version of this article.)

for PP increases. The CS becomes less important than PP above 10 MeV. In the PP, the number of DPA produced by positrons is 68%-77% of those induced by electrons. It is thus important to differently treat positrons and electrons in PP for damage calculations.

In the heavy reflector of PERLE experiment, 53.6% photons cannot induce displacement damage for iron due to the threshold of atomic displacement. The gamma-induced DPA rate can be computed with the corresponding DPA cross sections for a given gamma spectrum. Based on Monte Carlo simulations, the gamma-induced total damage rate in the reflector of PERLE is 9.8×10^{-10} DPA/year, which implicates about 8.1×10^{-4} DPA/year gamma-induced atomic displacement in the heavy reflector of EPR.

Acknowledgments

References

[1] R.E. MacFarlane, A.C. Kahler, Methods for processing ENDF/B-VII with NJOY, Nucl. Data Sheets 111 (12) (2010) 2739–2890.
[2] S. Chen, D. Bernard, P. Tamagno, J. Tommasi, S. Bourganel, and G. Noguere, "Irradiation Damage Calculation with Angular Distribution," arXiv, no. 1902.05620, 2019.
[3] S. Chen, D. Bernard, P. Tamagno, and C. De Saint Jean, "Calculation and Verification of Irradiation Damage Cross Section with Energy-Angular Distribution," arXiv, no. 1902.04889, 2019.
[4] S. Chen, D. Bernard, L. Buiron, Study on the self-shielding and temperature influences on the neutron irradiation damage calculations in reactors, Nucl. Eng. Des. 346 (2019) 85–96.
[5] M. Chenaud, et al., Status of the ASTRID core at the end of the pre-conceptual design phase 1, Nucl. Eng. Technol. 45 (6) (2013) 721–730.
[6] D.E. Alexander, L.E. Rehn, The contribution of high energy gamma rays to displacement damage in LWR pressure vessels, J. Nucl. Mater. 209 (2) (1994) 212–214.
[7] D.E. Alexander, L.E. Rehn, Gamma-ray displacement damage in the pressure vessel of the advanced boiling water reactor, J. Nucl. Mater. 217 (1) (1994) 213–216.
[8] O.S. Oen, D.K. Holmes, Cross sections for atomic displacements in solids by gamma rays, J. Appl. Phys. 30 (8) (1959) 1289–1295.

[9] O.S. Oen "Cross, sections for atomic displacements in solids by fast electrons", Oak Ridge National Laboratory Aug. 1973 Tennessee, US, ORNL-4897.
[10] N.F. Mott, The scattering of fast electrons by atomic nuclei, Proc. R. Soc. A 124 (794) (1929) 425–442.
[11] G.H. Kinchin, R.S. Pease, The displacement of atoms in solids by radiation, Rep. Prog. Phys. 18 (1) (1955) 1–51.
[12] N.P. Baumann "Gamma-ray Induced Displacements in D2O Reactors", in 1990 Strasbourg, France 9.
[13] J. Kwon, A.T. Motta, Gamma displacement cross-sections in various materials, Ann. Nucl. Energy 27 (18) (2000) 1627–1642.
[14] I. Piñera, et al., Improved calculation of displacements per atom cross section in solids by gamma and electron irradiation, Nucl. Instrum. Methods Phys. Res. Sect. B Beam Interact. Mater. At. 339 (2014) 1–7.
[15] M.J. Norgett, M.T. Robinson, I.M. Torrens, A proposed method of calculating displacement dose rates, Nucl. Eng. Des. 33 (1) (1975) 50–54.
[16] D.E. Alexander, Defect production considerations for gamma ray irradiation of reactor pressure vessel steels, J. Nucl. Mater. 240 (3) (1997) 196–204.
[17] K. Fukuya, I. Kimura, Calculation of gamma induced displacement cross-sections of iron considering positron contribution and using standard damage model, J. Nucl. Sci. Technol. 40 (6) (2003) 423–428.
[18] A. Santamarina et al., "The PERLE experiment for the qualification of PWR heavy reflectors," in Proc. of Int. Conf. on the Physics of Reactors: Nuclear Power: A Sustainable Resource (PHYSOR2008), Interlaken, Switzerland, 2008.
[19] C. Vaglio-Gaudard, et al., Interpretation of PERLE experiment for the validation of iron nuclear data using monte carlo calculations, Nucl. Sci. Eng. 166 (2) (2010) 89–106.
[20] S. Chen, C. Yuan, Neutronic analysis on potential accident tolerant fuel-cladding combination U3Si2-FeCrAl, Sci. Technol. Nucl. Install. 2017 (3146985) (2017).
[21] S. Chen, C. Yuan, D. Guo, Radial distributions of power and isotopic concentrations in candidate accident tolerant fuel U3Si2 and UO2/U3Si2 fuel pins with FeCrAl cladding, Ann. Nucl. Energy 124 (2019) 460–471.
[22] H. Bethe, Zur theorie des durchgangs schneller korpuskularstrahlen durch materie, Ann. Phys. 397 (3) (1930) 325–400.
[23] H.A. Bethe, J. Ashkin, Experimental Nuclear Physics vol. 1, John Wiley & Sons, New York, 1953.
[24] H. Cember, Introduction to Health Physics. New York, 1983.
[25] S.M. Seltzer, M.J. Berger, Evaluation of the collision stopping power of elements and compounds for electrons and positrons, Int. J. Appl. Radiat. Isot. 33 (11) (1982) 1189–1218.
[26] H.O. Wyckoff et al., "Stopping Powers for Electrons and Positrons," International Commission on Radiation Unit and measurements, MD. 20814, USA, ICRU Report 37, Oct. 1984.
[27] W.A. McKinley, H. Feshbach, The coulomb scattering of relativistic electrons by nuclei, Phys. Rev. 74 (12) (1948) 1759–1763.
[28] K. Nordlund, J. Wallenius, L. Malerba, Molecular dynamics simulations of threshold displacement energies in Fe, Nucl. Instrum. Methods Phys. Res. Sect. B Beam

Interact. Mater. At. 246 (2) (2006) 322–332.

[29] J. Lindhard, V. Nielsen, M. Scharff, P.V. Thomsen, Integral equations governing radiation effects, Mat Fys Medd Dan Vid Selsk 33 (10) (1963) 1–42.

[30] M.T. Robinson, Energy dependence of neutron radiation damage in solids, Nucl. Fusion React. (1970) 364–378.

[31] O. Klein, Y. Nishina, Über die streuung von strahlung durch freie elektronen nach der neuen relativistischen quantendynamik von dirac, Z. Für Phys. 52 (11) (Nov. 1929) 853–868.

[32] C.M. Davisson, R.D. Evans, Gamma-ray absorption coefficients, Rev. Mod. Phys. 24 (2) (1952) 79–107.

[33] R.D. Evans, The Atomic Nucleus, McGraw-Hill, New York, 1955.

[34] E. Brun, et al., TRIPOLI-4*, CEA, EDF and AREVA reference Monte Carlo code, Ann. Nucl. Energy 82 (2015) 151–160.

[35] D. E. Cullen, J. H. Hubbell, and L. Kissel, "EPDL97: the Evaluated Photon Data Library, '97 Version," Lawrence Livermore National Laboratory, Livermore, US, UCRL-LR-50400 Vol 6 Rev 5, Sep. 1997.

[36] A. Santamarina et al. "The JEFF-3.1.1 Nuclear Data Library", OECD/NEA, JEFF Report 22 NEA No. 6807, 2009.